

Evaluation-Strategy Gap in Fault Diagnosis of Deep Learning Programs

Sigma Jahan

Faculty of Computer Science
Dalhousie University, Halifax, Canada
sigma.jahan@dal.ca

Abstract—Deep Learning (DL) programs can fail during training for many reasons, and diagnosing the cause is a costly and time-consuming maintenance task. Techniques for diagnosing such failures are commonly assessed using within-program cross-validation, which may be inadequate for deployment settings involving previously unseen programs. It is therefore necessary to assess how performance differs across these settings and to identify the causes of any performance gap in established fault diagnosis techniques for DL. We investigate this gap using DYNFAULT, a corpus of 5,542 fault-injected training traces from 38 real-world DL programs. We found a gap of 0.190 in balanced accuracy for existing fault diagnosis techniques between within-program evaluation and holding out whole programs. We also found the gap comes from program-level structure in the features, which led us to examine two runtime feature sets, curvature features and optimizer features, and their behavior on unseen programs. We found that curvature features are useful for instability detection on unseen programs, while optimizer and activation features help only on programs seen during training.

Index Terms—deep learning, dynamic analysis, fault diagnosis, generalization, program-held-out evaluation

I. INTRODUCTION

Deep Learning (DL) programs are prone to training-time failures caused by configuration errors, implementation bugs, and numerical instability [1], [2]. Diagnosing these failures is challenging, as DL programs can vary widely in architecture, data set, and training configuration. The loss landscape, the dynamics of the gradients and the convergence behavior of one program can differ substantially from another [3]. When a training run diverges, overfits, or shows inconsistent training and validation behavior, practitioners must diagnose the root cause from available information (e.g., runtime metrics, code snippets, model outputs), often under tight time and compute budgets [4], [5]. Fault diagnosis techniques based on dynamic analysis learn to identify such failures by observing runtime signals (e.g., loss trajectories, gradient statistics, and optimizer states) [6], [7], [8], [9].

Existing fault diagnosis techniques often report strong results under cross-validation within the program, and several also validate on a limited number of real-world fault benchmarks. For these techniques, each program produces characteristic patterns in runtime metrics, so a classifier trained in one set of programs can learn to identify those programs instead of faults [10]. Within-program splits put the same programs in training and testing, and fixed benchmarks report one aggregate score. Neither approach measures the impact on the

performance of fault diagnosis for entirely new DL programs. Systematic evaluation on excluded groups is common practice in cross-project defect prediction [11], [12] as well as grouped cross-validation for clustered data [13], [14]. However, similar evaluation strategies have not been widely adopted for fault diagnosis techniques that learn from runtime data, leading to two major gaps, as follows.

The impact of evaluation strategy on fault diagnosis remains unclear. We have limited systematic evidence on how much the performance of existing fault diagnosis techniques changes under different evaluation strategies, since previous work often overlooks these evaluation setups. A decline in performance could indicate that the fault signal does not transfer or that within-program evaluation partly rewards a classifier for recognizing the program rather than the fault [9]. These explanations imply different causes for the observed decline, which cannot be identified from the performance drop alone. Thus, more comprehensive evaluation and analysis are warranted to understand how the performance of fault diagnosis techniques reflects the overall diagnostic capability.

The value of runtime features remains unclear across evaluation strategies. Existing fault diagnosis techniques differ in terms of the runtime metrics collected to learn fault patterns [6], [7], [8], [15], [16]. Richer instrumentation is often necessary to collect these metrics, which can be costly. However, it remains unclear whether the choice of evaluation strategy affects the usefulness of these runtime metrics. Thus, it is difficult to weigh the cost of richer logging against its likely benefit for unseen programs.

To address these gaps, we study DYNFAULT, a corpus of 5,542 fault-injected training traces from 38 real-world DL programs to compare two ways of splitting the data. In *within-program* evaluation, runs are split without regard to which program they came from. In *program-held-out* evaluation, all runs from a given program stay together, so a tested program never appears in training. We examine three diagnostic tasks, (a) fault-type classification, (b) catastrophic-instability triage, and (c) training/validation mismatch detection. In each task, we also compare two runtime feature configurations, first-order optimizer and activation features, and second-order curvature features built from Hessian-vector products (HVPs). In short, we ask the following research questions.

- **RQ₁: How large is the within-program vs. program-held-out gap for fault-type diagnosis, and what causes**

it? We measure the gap on the four-class fault-type task and then run four controls (program-identity prediction, label permutation, per-program normalization, and distribution-level shift analysis). These controls trace the gap to program-level structure in the features.

- **RQ₂: When does catastrophic instability occur, and do curvature features detect it on unseen programs?** We find that instability occurs at initialization, before substantial training has taken place, and that curvature features improve detection on new programs at every observation window. They provide an instability signal that transfers.
- **RQ₃: Do optimizer features generalize for training/validation mismatch detection?** We find that optimizer and activation features improve mismatch detection within a program but lose much of that benefit on new programs. The extra logging adds accuracy that does not transfer, and within-program evaluation hides the loss.

We release DYNFAULT and the full evaluation framework as a replication package [17]. Table I positions our study within existing fault diagnosis research and shows that program-held-out evaluation is rarely reported for learning-based techniques.

TABLE I
FAULT DIAGNOSIS TECHNIQUES FOR DL PROGRAMS AND THEIR EVALUATION SCOPE

Technique	Approach	Categories	Signals	Prog-held-out	Split
DeepFD [7]	kNN/DT/RF	5 types	Runtime	×	Within
Qi et al. [9]	RF	5 types	Runtime, coverage	×	Within
AutoTrainer [15]	Rules	5 problems	Runtime	—	Within
DeepDiagnosis [6]	Rules + DT	8 symptoms	Runtime	—	Within
DEFault [8]	Hierarchical RF	7 types	Runtime, static	×	Within
Our study	LR	4–6 types	Runtime (CF, OF)	✓	Both

✓ evaluated under a program-held-out split, × not reported, — not applicable (rule-based detectors). *Categories* are the distinct fault types, training problems, or symptoms a technique reports. *Signals*: runtime = per-epoch training metrics (e.g., loss, accuracy, gradient, weight). Coverage = neuron-coverage metrics. Static = code-structure features. CF & OF = curvature and optimizer feature sets. Parenthesized numbers are reported feature counts. *Approach*: kNN, DT = decision tree, RF = random forest, LR = logistic regression.

II. BACKGROUND AND CORPUS

A. Dynamic Analysis Techniques for Fault Diagnosis

Dynamic analysis techniques learn from per-epoch scalar metrics of a training run, such as loss, accuracy, and gradient statistics, to classify fault types or recommend corrective actions [6], [7], [8], [9]. Existing work evaluates under within-program splits and, in several cases, on separate real-world fault benchmarks, but does not isolate how performance changes on a previously unseen program. Our study addresses this dimension between programs by separately characterizing two maintenance scenarios. Within-program reuse applies a model to new runs of a program already in the training data, and cross-program deployment applies it to a program not seen during training.

B. The DYNFAULT Corpus

DYNFAULT is a corpus of 5,542 labeled training traces constructed for this study. Each trace is a per-epoch CSV

of scalar training metrics produced by a mutation-injected run of one of 38 distinct real-world DL programs (FFNN, RNN, and CNN architectures). Each program is identified by its Stack Overflow post identifier (`so_id`).

Baseline of the program and the mutation protocol.

38 DL programs are real-world examples curated from Stack Overflow [8]. We inject faults using the extended set of mutation operators, covering seven major fault categories based on empirical studies of real DL bugs [1], [8], [18], [19]. These categories are hyperparameter, loss function, activation, layer configuration, optimizer, weight initialization, and regularization. We classify each mutant as killed or survived using the Generalized Linear Model (GLM) criterion [20] from previous work [8], [19]. Mutants that are killed are assigned a fault label that reflects their mutation category. The Weight-initialization mutants did not produce killed runs, thus six of the seven categories appear in our labeled corpus.

Runtime feature configurations. Prior diagnosis techniques use standard metrics such as loss, accuracy, and gradient statistics [6], [7], [8]. DYNFAULT also includes curvature metrics derived from Hessian-vector products (HVPs) [21], motivated by evidence that Hessian-derived metrics can localize training instability and fault sources in DL programs [22]. The optimizer-feature configuration adds optimizer control-state and activation extrema metrics that gradient norms alone do not capture. We record the two configurations separately and treat them as alternative runtime feature designs (Section II-C).

Scope. We use DYNFAULT to measure how evaluation strategy and runtime feature set jointly determine diagnostic performance and generalizability (Table II). Mutation injection gives every trace a known label and a reproducible fault condition. This controlled design isolates evaluation bias and limits our conclusions to the injected-fault corpus.

TABLE II
CORPUS COMPOSITION OF DYNFAULT

Item	Count	Notes
Total trace files	5,542	One CSV per mutated run
Non-empty runs	4,980	At least one epoch row recorded
Crash-before-epoch	562	Header only, no epoch data
Distinct programs	38	Unique program identifiers
CF runs	4,175	Curvature feature set
OF runs	1,367	Optimizer feature set
Unstable runs	219	Loss > 10 ⁶ , 4.4% of non-empty
Fault categories (runs / programs)		
Activation	90	2 programs
Hyperparameter	1,357	22 programs
Layer	2,802	38 programs
Loss function	991	14 programs
Optimization	267	14 programs
Regularization	35	1 program

CF = curvature feature set (HVP-based), OF = optimizer & activation feature set.

C. Two Runtime Feature Sets

The runtime feature configuration determines what a trace contains and which failure modes can be diagnosed. Adding

HVP logging or extreme activation recording can make a previously trained diagnostic model inapplicable, since the model expects a different set of input features. We study two configurations present in DYNFAULT.

Curvature features. Curvature proxies are derived from the Hessian of the loss with respect to model parameters,

$$H = \nabla_{\theta}^2 \mathcal{L}(\theta) \quad (1)$$

where \mathcal{L} is the training loss and θ denotes the parameter vector. Forming H explicitly is prohibitive for large networks, so practical implementations use Pearlmutter’s R -operator [23], a differential operator that propagates directional derivatives through the computation graph. The R -operator computes HVP in $\mathcal{O}(|\theta|)$ time via one additional forward-backward pass.

$$Hv = \nabla_{\theta}[(\nabla_{\theta}\mathcal{L})^{\top}v] \quad (2)$$

From the per-layer HVP vectors we extract scalar summaries, the mean μ_{HVP} and standard deviation σ_{HVP} , together with per-layer HVP norms $\|Hv\|_2$. These curvature metrics are used in curvature-aware optimization [24] and have been linked to training instability at the edge of stability, where the largest Hessian eigenvalue hovers near $2/\eta$ [25], [26], [27]. Prior work shows that they localize fault sources in attention-based architectures more effectively than gradient norms alone [22].

Optimizer features. Optimizer features capture first-order gradient statistics and control-state metrics. Global gradient norm,

$$\|\nabla_{\theta}\mathcal{L}\|_2 = \sqrt{\sum_i \left(\frac{\partial\mathcal{L}}{\partial\theta_i}\right)^2} \quad (3)$$

summarizes the overall magnitude of the update at each training step. In addition, we record the current learning rate η_t , per-layer activation statistics (mean μ_{act} , standard deviation σ_{act}), gradient extrema ($\max|\nabla_{\theta}\mathcal{L}|$, $\min|\nabla_{\theta}\mathcal{L}|$), and system resource metrics. These metrics are available in current training debuggers and monitoring dashboards [16], [28]. Table III lists the runtime metrics recorded under each configuration. Section III-C describes the summary statistics derived from each metric.

Table III lists the global runtime channels shared across the two feature configurations. The instability analyses additionally include per-layer and profile summaries derived from these channels. The feature counts in Table VI therefore exceed the channel counts shown here.

III. METHODOLOGY

We outline the diagnostic tasks, feature extraction procedures, and evaluation protocols in Fig. 1.

A. Analysis Subsets

All learning-based analyses require epoch-level metrics. We therefore restrict to *non-empty* traces (Table II) that contain at least one logged epoch row. The 562 crash traces fall predominantly in Layer (355) and Hyperparameter (131), the two largest categories, with the rest in Loss (46), Optimization (19), and Activation (11). Their exclusion does not appear to

TABLE III
RUNTIME METRICS PER FEATURE CONFIGURATION

Group	Metric	CF	OF
Performance	Training loss	✓	✓
	Validation loss	✓	✓
	Training accuracy	✓	✓
	Validation accuracy	✓	✓
Curvature	Mean HVP (μ_{HVP})	✓	—
	HVP standard deviation (σ_{HVP})	✓	—
Gradient	Mean gradient	—	✓
	Gradient standard deviation	—	✓
	Gradient extrema (min, median, max)	—	✓
Optimizer / activation	Learning rate (η_t)	—	✓
	Activation mean (μ_{act})	—	✓
	Activation standard deviation (σ_{act})	—	✓
System resources	CPU usage	—	✓
	GPU memory usage	—	✓
	System memory usage	—	✓

✓ recorded, — not recorded. CF: 6 metrics (4 performance + 2 curvature). OF: 15 metrics (4 performance + 11 optimizer and system). HVP = Hessian-vector product.

materially distort the fault-category distribution. Some analyses use configuration-specific subsets. Curvature-feature (CF) and optimizer-feature (OF) traces were collected for different sets of programs. When comparing absolute performance across CF and OF, we either (i) restrict to the subset of programs that appear under both feature configurations (overlap-controlled comparison), or (ii) compare *within-configuration* generalizability gaps under the same feature configuration.

B. Diagnostic Tasks

1) *Fault-type classification:* We predict the mutation category of a trace at three granularities: (i) six-class fault type, (ii) four-class core fault type, and (iii) three-class fault family. This task is the primary subject of RQ1. Program-held-out evaluation requires training examples for each class in every fold, so we treat the four-class task as the primary cross-program estimate (Section IV-A).

2) *Catastrophic instability triage:* We label a trace as *unstable* if the training or validation loss exceeds 10^6 at any logged epoch. This threshold captures unambiguous numerical divergence. Under standard cross-entropy losses, a value of 10^6 corresponds to predicting near-zero probability for the true class across batches, a condition that is generally not recoverable in practice. A sensitivity check at thresholds 10^3 and 10^4 shows that the epoch-0 concentration result holds (Section IV-B).

3) *Training/validation performance mismatch detection (T/V-mismatch):* We label a stable trace as a *T/V-mismatch* case if the per-epoch boolean flag `acc_gap_too_big` is true in at least one epoch of the observed window. The flag is set at each epoch e when the absolute training–validation accuracy gap meets or exceeds 0.1 (10%):

$$\text{acc_gap_too_big}_e = 1[|\text{acc}_{\text{train},e} - \text{acc}_{\text{val},e}| \geq 0.1]. \quad (4)$$

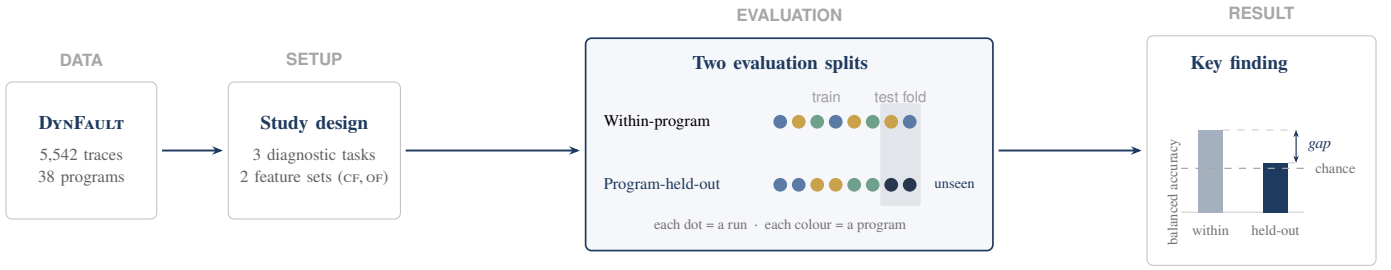


Fig. 1. Study design overview

This threshold and computation rule originate from the DEFault corpus construction protocol [8] and are applied identically (see our replication package [17]). To isolate mismatch effects from catastrophic failures, we restrict this task to stable traces only (i.e., no loss explosion in any epoch).

C. Feature Extraction

For each scalar metric channel z_e observed over the first k logged epochs $e \in \{0, \dots, k-1\}$, we extract two summary statistics: the window mean \bar{z}_k and the ordinary least-squares slope $\hat{\beta}_k$,

$$\bar{z}_k = \frac{1}{k} \sum_{e=0}^{k-1} z_e, \quad \hat{\beta}_k = \frac{\sum_{e=0}^{k-1} (e - \bar{e})(z_e - \bar{z}_k)}{\sum_{e=0}^{k-1} (e - \bar{e})^2}, \quad (5)$$

where $\bar{e} = (k-1)/2$. For a trace with d scalar channels, the feature vector at observation window k is $\mathbf{x}_k \in \mathbb{R}^{2d}$ formed by concatenating the mean and slope for each channel. When $k=1$, the slope term is undefined, so we use only the mean statistics at $k=1$, giving d features. We consider observation windows $k \in \{1, 3, 5, 10, 20, 50\}$. We standardize features using statistics from the training split only and clip values to $[\pm 10^{12}]$. Missing channels are imputed with column medians computed on the training split.

We use logistic regression with class-balanced weights and a one-vs-rest formulation for multi-class tasks. This setting provides a controlled linear probe of the feature representation under each evaluation protocol, keeping classifier capacity fixed while comparing within-program and program-held-out splits. Although logistic regression is linear, it can still capture program-level differences when those differences are present in the features. We use it to test whether the evaluation gap appears even without a high-capacity classifier. For comparisons with existing fault diagnosis techniques [7], [8], we report their original Random Forest classifiers alongside logistic regression (Section IV-C). On the same DEFault feature set, the gap widens from 0.088 under logistic regression to 0.34 under random forest (Fig. 13), so the logistic-regression gap we report for RQ1 is the conservative estimate. Logistic regression also enables the per-fold coefficient analysis in Fig. 11 that a random-forest ensemble would mask.

D. Evaluation Strategies

1) *Within-program evaluation*: We perform stratified K -fold cross-validation over individual runs ($K=5$). Runs from

the same program may appear in both training and test folds. This protocol measures *within-program reuse*, where a trained diagnostic model is applied to new runs of a program already represented in training data.

2) *Program-held-out evaluation*: We perform grouped K -fold cross-validation over runs ($K=5$) with program identifiers as the grouping variable, so that each test fold contains only programs entirely absent from the corresponding training fold. This protocol measures *cross-program deployment*, where a model is applied to a program not seen during training. For the cluster-based curvature triage heuristic (Algorithm 1), we additionally report a stricter leave-one-program-out (LOPO) evaluation that holds out each program in turn. We use LOPO because the heuristic is trained without labels and produces a single interpretable “terminate” action, for which per-program precision is directly interpretable.

3) *Metrics and uncertainty*: For multi-class tasks we report balanced accuracy. Unless otherwise noted, “accuracy” refers to *balanced accuracy throughout this paper*. For binary tasks we report ROC-AUC and PR-AUC. PR and ROC curves pool out-of-fold predicted probabilities across folds. We compute 95% confidence intervals via a cluster bootstrap over programs (with replacement) [29], preserving within-program dependence.

4) *Evaluation-strategy gap*: Let $M_{\text{within}}(k)$ and $M_{\text{heldout}}(k)$ denote the value of a metric M obtained under within-program and program-held-out evaluation, respectively, for the same classifier and feature vector \mathbf{x}_k . The *evaluation-strategy gap* is

$$\Delta_M(k) = M_{\text{within}}(k) - M_{\text{heldout}}(k). \quad (6)$$

A positive $\Delta_M(k)$ indicates that within-program evaluation reports a higher figure than program-held-out evaluation at k observed epochs.

E. Evaluation-Strategy Controls

We use three classifier-based controls to identify the source of the within-program advantage.

1) *Program-identity prediction*: We predict the program identifier from early-epoch features. High accuracy indicates that feature vectors encode program-level structure beyond fault semantics.

2) *Within-program label permutation*: We randomly permute fault labels *within each program*, preserving each program’s label frequencies, and re-evaluate under within-program

TABLE IV
EVALUATION-STRATEGY GAP AT $k=5$

Task	Classes	Chance	Within-prog.	Cross-prog.	Gap
Fault type	4	0.25	0.469 [0.343, 0.545]	0.279 [0.232, 0.319]	0.190 [0.053, 0.258]
Fault type	6	0.17	0.468 [0.310, 0.500]	0.178 [0.160, 0.281]	0.290 [0.091, 0.325]
Fault family	3	0.33	0.518 [0.446, 0.595]	0.391 [0.346, 0.438]	0.128 [0.043, 0.206]

Shaded row is the primary four-class estimate. Values are balanced accuracy with 95% bootstrap confidence interval in brackets. Chance = 1/(number of classes). The six-class row is reported for completeness.

cross-validation. Above-chance performance after permutation indicates that within-program evaluation can succeed using program-level structure even when fault labels carry no discriminative information.

3) *Per-program normalization (analysis-only control)*: As an analysis-only control (i.e., not deployable in practice), we z -normalize features within each program (i.e., subtract the per-program mean and divide by the per-program standard deviation) *before* any cross-validation split, since this uses unlabeled information from the held-out programs. If within-program performance drops substantially while program-held-out performance changes little, the evaluation gap is driven by program-level feature statistics rather than transferable fault signal.

IV. STUDY FINDINGS

A. Evaluation-Strategy Gap

Answering RQ₁: The within-program vs. program-held-out gap and its cause

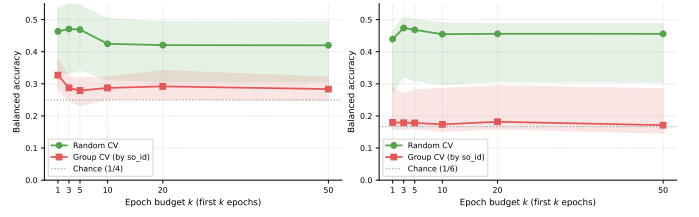
To answer RQ₁, we measure the within-program and program-held-out balanced accuracy for fault-type classification, and then apply four controls to identify what produces any difference between them.

Table IV reports accuracy at $k=5$, a representative early-epoch window. The full analysis across all k values is in our replication package [17]. We treat the four-class task (Layer, Hyperparameter, Loss, Optimization) as the primary estimate because each class appears in at least 14 programs, making program-held-out evaluation well-defined. The six-class task adds Activation (2 programs) and Regularization (1 program), so some program-held-out folds lack training signal for those labels. We report it for completeness and interpret its near-chance cross-program accuracy accordingly. This near-chance result ($0.178 \approx 0.17$ chance) reflects the sparse program coverage for these two categories rather than a genuine absence of transferable signal.

On the four-class task, within-program accuracy is 0.469 [0.343, 0.545] and cross-program accuracy is 0.279 [0.232, 0.319], a gap of 0.190 [0.053, 0.258]. In our experiments, the program-held-out score is only slightly higher than the 0.25 chance baseline, and its 95% CI includes chance-level performance. We therefore interpret this result as limited cross-program fault-type discrimination in this corpus, rather than deployment-ready diagnosis. The main empirical finding is the drop from within-program to program-held-out

evaluation. Our control experiments suggest that this drop is partly explained by program-specific patterns in the runtime features.

Fig. 2 shows that this separation between within-program and program-held-out evaluation holds across all observation windows k on both task granularities. The primary four-class task preserves a positive gap at every k . On the six-class task the gap ranges from approximately 0.13 at $k=1$ to 0.29 at $k=50$, with the lower bound exceeding zero throughout (the minimum CI lower bound is 0.044, at $k=1$), so the gap is not explained by the observation window alone. We next use three classifier-based controls and one distribution-level analysis to identify its source.

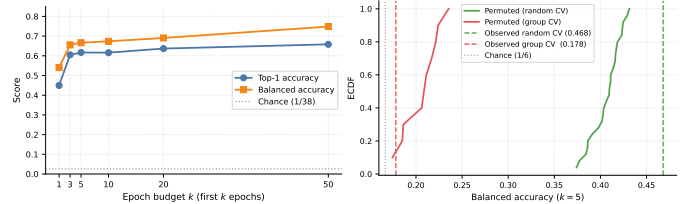


(a) Four-class fault type

(b) Six-class fault type

Fig. 2. Evaluation-strategy gap across observation windows k

(a) *Program-identity predictability*. Fig. 3a shows that 38-class program-identity accuracy reaches 0.62 at $k=5$ (chance is 0.026), rising monotonically with k . We observed that a diagnostic model operating on these features can identify the program independently of fault labels, suggesting that program-level structure contributes to within-program CV performance.



(a) Predict program identity

(b) Within-program accuracy

Fig. 3. Program-level structure controls at $k=5$

(b) *Within-program label permutation*. Fig. 3b shows that permuting fault labels within each program keeps within-program CV accuracy well above chance. Across 25 permutations, median permuted accuracy is 0.41, versus a 0.17 chance baseline (6-class uniform) and 0.47 for the unpermuted case. We found that a classifier achieves accuracy well above chance on within-program splits even when fault labels carry no discriminative information, suggesting that program-level structure in the feature space contributes to this performance independently of fault-label content.

(c) *Per-program normalization*. Table V shows the normalization control. After z -normalizing features within each program, program-identity accuracy drops from 0.617 to 0.096 and within-program fault-type accuracy from 0.468 to 0.325,

while cross-program accuracy remains similar (0.178 to 0.158), indicating that the within-program drop reflects removal of program-level shortcuts rather than loss of generalizable signal.

TABLE V
PER-PROGRAM NORMALIZATION CONTROL AT $k=5$

Metric	Setting	Raw	Normalized	Δ
Fault-type accuracy	within	0.468 [0.310, 0.500]	0.325 [0.229, 0.473]	-0.143
	cross	0.178 [0.160, 0.281]	0.158 [0.129, 0.269]	-0.020
Program-identity accuracy	within	0.617	0.096	-0.521

Values are balanced accuracy with 95% confidence interval in brackets (program-identity is plain accuracy). Δ = normalized - raw.

(d) *Distribution-level domain shift.* The controls above use classifier accuracy as a proxy for program-level structure. For a distribution-level analysis, we compute the pairwise Maximum Mean Discrepancy (MMD, RBF kernel with median heuristic bandwidth) [30] between the feature distributions of all 38 programs at $k=5$ using the four shared performance channels (loss and accuracy, mean and slope). The median pairwise MMD² across all 703 program pairs is 0.716, with a mean of 0.774 and a range of 0.0 to 1.93. Under the RBF kernel with median heuristic bandwidth, MMD² is 0 for identical distributions and increases without a fixed upper bound as distributions diverge. A value of 0.716 therefore reflects substantial inter-program separation. Fig. 4 shows the heatmap sorted by mean domain shift. The large inter-program distances suggest that programs occupy distinct feature-space regions, consistent with the program-identity prediction in control (a).

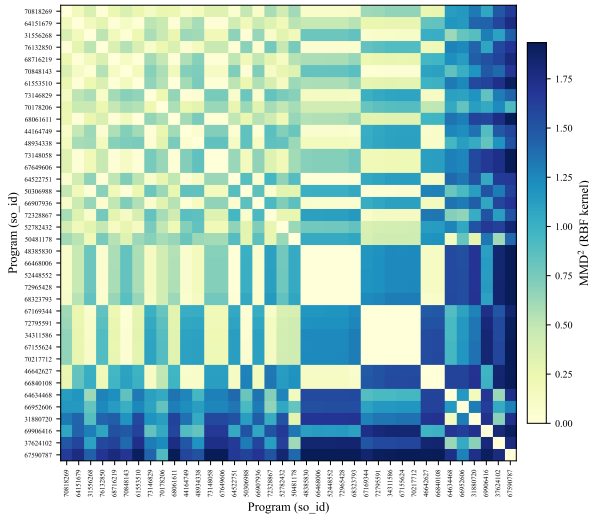


Fig. 4. Pairwise MMD² between program feature distributions at $k=5$

All four controls point to the same explanation. The within-program CV advantage is attributable to program-level structure in the feature space rather than transferable fault semantics. This structure is visible at the distribution level (median pairwise MMD² 0.716), predictable by a classifier (62% program-identity accuracy), exploitable even under permuted labels

(accuracy 0.41 vs. chance 0.17), and removable by per-program normalization without affecting cross-program performance. Within-program evaluation remains valid as a measure of reuse performance, and the two strategies capture different signals and should be interpreted accordingly. The remaining questions examine which runtime features and diagnostic tasks remain effective under the harder cross-program standard.

RQ₁ Summary. We found that within-program fault-type accuracy exceeds cross-program accuracy by 0.190 at $k=5$. Four converging controls confirm that program-level feature structure, rather than fault signal, accounts for this gap. These results show that within-program evaluation substantially overstates diagnostic ability.

B. Runtime Feature Generalizability

Answering RQ₂: Instability timing and curvature-based detection on unseen programs

To answer RQ₂, we first determine when catastrophic instability occurs during training, and then test whether adding curvature features improves its detection on unseen programs.

Instability timing. Fig. 5a shows the distribution of the first epoch of loss explosion across all 219 unstable runs. Of these, 96% (211 of 219) explode at epoch 0 and 98% (214) by epoch 1. We found that this concentration holds across the instability threshold. At thresholds 10^3 and 10^4 , 99.0% and 91.9% of unstable runs, respectively, first explode at epoch 0 (vs. 96.3% at 10^6). Lowering the threshold increases the flagged set (11.9% of runs at 10^3 and 6.9% at 10^4 , vs. 4.4% at 10^6), so 10^6 is the most conservative threshold. These results indicate that, in our dataset, instability monitoring is most informative at initialization, before substantial training compute is spent.

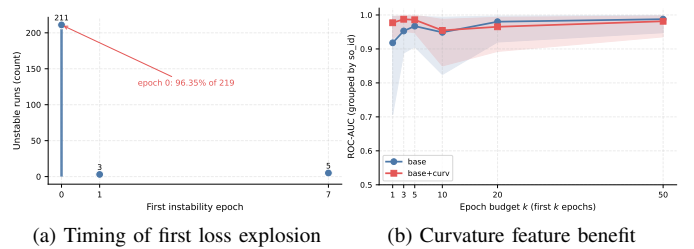


Fig. 5. Instability characterization (a) 96% of unstable runs explode at epoch 0 (b) adding curvature features improves cross-program detection at every k

Curvature feature addition. Table VI reports instability detection under program-held-out evaluation for baseline features and baseline combined with curvature features. At $k=1$, adding curvature features improves ROC-AUC from 0.918 [0.707, 0.996] to 0.977 [0.930, 0.995]. The loss-ablated variants suggest that this gain is not explained solely by rising loss values. In our study, curvature provided an additional early indicator of instability. PR-AUC confidence intervals are wide at the 4.4% positive rate, because cluster-bootstrap resampling can produce folds with very few unstable runs, so ROC-AUC is the primary metric. Figure 5b shows curvature benefit across all k .

TABLE VI
CROSS-PROGRAM INSTABILITY DETECTION

Feature set	k	#Features	ROC-AUC	PR-AUC
Baseline	1	19	0.918 [0.707, 0.996]	0.776 [0.466, 0.956]
Baseline	5	38	0.967 [0.906, 0.996]	0.768 [0.635, 0.954]
Baseline + CF	1	22	0.977 [0.930, 0.995]	0.896 [0.700, 0.977]
Baseline + CF	5	43	0.986 [0.948, 0.999]	0.894 [0.752, 0.991]
No-loss baseline	1	17	0.850 [0.566, 0.966]	0.547 [0.181, 0.911]
No-loss baseline	5	34	0.954 [0.888, 0.988]	0.601 [0.345, 0.899]
No-loss + CF	1	20	0.896 [0.743, 0.966]	0.756 [0.312, 0.916]
No-loss + CF	5	39	0.950 [0.865, 0.980]	0.684 [0.325, 0.930]

Program-held-out evaluation, values with 95% confidence interval in brackets. ROC-AUC and PR-AUC = area under the ROC & precision-recall curves.

Cross-program risk stratification. Fig. 6 reports instability prevalence by quintile of mean HVP and gradient standard deviation at epoch-0. We observed that both metrics exhibit a consistent risk gradient across quintiles, which suggests that they may support a cross-program triage heuristic without a trained classifier. Fig. 7 shows the underlying pattern, where unstable runs exhibit uniformly elevated HVP magnitude across all network layers (median ≈ 0.7 log units above stable runs), suggesting that loss-surface curvature at initialization may be a whole-network property rather than a layer-specific artifact.

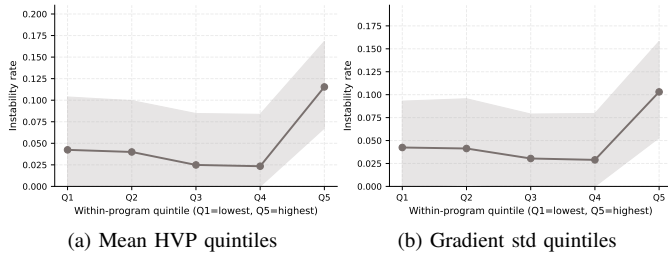


Fig. 6. Instability rate by epoch-0 quintile

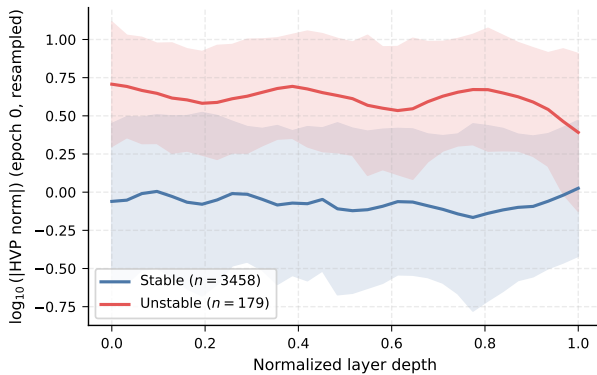


Fig. 7. Layer-wise HVP magnitude at epoch 0

Curvature-based triage rule. We also examined whether epoch-0 curvature geometry can group runs into interpretable categories before training proceeds. We cluster the 3,637

TABLE VII
CURVATURE CLUSTER PATTERNS

Cluster	n	Programs	Unstable (%)	Mismatch (%)	Median HVP	Median ∇ -std
0	1346	19	0.5	49.1	6.1×10^{-1}	1.4×10^{-2}
1	121	9	100.0	3.3	5.4×10^6	6.8×10^5
2	367	8	0.8	28.6	6.4×10^{-1}	8.8×10^{-2}
3	100	4	10.0	0.0	9.2×10^3	1.0×10^4
4	536	6	2.2	0.9	1.9×10^{-1}	1.5×10^{-2}
5	933	17	1.9	50.2	5.2×10^{-2}	1.4×10^{-2}
6	234	8	3.4	8.5	4.0×10^1	1.8×10^1

$K=7$ partition of 3,637 epoch-0 curvature-feature runs. n = runs in cluster, ∇ -std = gradient standard deviation, HVP = Hessian-vector product. Low-curvature clusters (C0, C4, C5) show near-zero instability but differ sharply in mismatch prevalence.

curvature-feature runs by epoch-0 curvature geometry (HVP magnitude, gradient standard deviation, per-layer profile summaries) using k -means. Average silhouette coefficients peak at $K=2$ (0.742), indicating a dominant split between high-curvature and low-curvature runs. For the phenotype analysis we fit a finer $K=7$ partition over all 3,637 curvature-feature runs (Table VII, Fig. 8), which resolves outcome variation inside the low-curvature majority while keeping the extreme high-curvature cluster. The three largest low-curvature clusters (C0, C4, C5) share near-zero instability rates but differ sharply in mismatch prevalence. Table VII summarizes each cluster and Fig. 8 shows the PCA embedding.

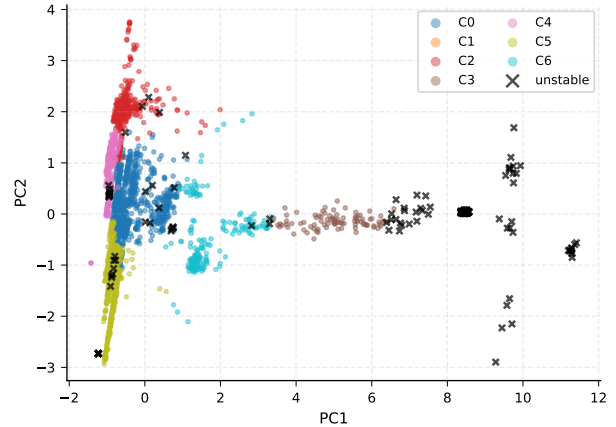


Fig. 8. PCA of epoch-0 curvature features by cluster ($K=7$)

Zero-false-positive early-termination rule. Cluster C1 ($n=121$, median mean HVP 5.37×10^6 , 9 programs) is 100% unstable. Treating C1 membership as a termination signal achieves precision 1.00, recall 0.676, and F1 0.807 on the 179 unstable curvature-feature runs in the full in-sample evaluation. Of these, 121 runs can be terminated at epoch 0 with zero false positives.

Evaluation protocol distinction. The supervised instability models in Table VI use *program-held-out grouped 5-fold cross-validation* (Section III-D). The triage heuristic below uses a stricter *leave-one-program-out* (LOPO) protocol because it is unsupervised and produces a single binary “terminate” action for which per-program precision is directly interpretable. Grouped 5-fold provides aggregate metrics with bootstrap

Algorithm 1. LOPO Curvature Triage

Input: Epoch-0 CF vectors $\{\mathbf{x}_0^{(i)}\}$, program labels $\{p^{(i)}\}$, instability labels $\{y^{(i)}\}$, clusters K

Output: LOPO precision and recall

TP \leftarrow 0;
 FP \leftarrow 0;
 FN \leftarrow 0;

foreach unique program $p \in \mathcal{P}$ **do**

$\mathcal{D}_{\text{train}} \leftarrow \{\mathbf{x}_0^{(i)} : p^{(i)} \neq p\}$;
 $\mathcal{D}_{\text{test}} \leftarrow \{\mathbf{x}_0^{(i)} : p^{(i)} = p\}$;
 $\{\mu_1, \dots, \mu_K\} \leftarrow k\text{-means}(\mathcal{D}_{\text{train}}, K)$;
 $c^* \leftarrow \arg \max_j \mu_j [\text{mean-HVP}]$ // highest mean-HVP centroid;

foreach $(\mathbf{x}_0^{(i)}, y^{(i)}) \in \mathcal{D}_{\text{test}}$ **do**

$j^* \leftarrow \arg \min_j \|\mathbf{x}_0^{(i)} - \mu_j\|_2$;

if $j^* = c^*$ **then**

TERMINATE;

if $y^{(i)} = 1$ **then** TP \leftarrow TP + 1;

else FP \leftarrow FP + 1;

else

CONTINUE;

if $y^{(i)} = 1$ **then** FN \leftarrow FN + 1;

TP

return $\frac{\text{TP}}{\text{TP} + \text{FP}}, \frac{\text{TP}}{\text{TP} + \text{FN}}$;

confidence intervals. LOPO characterizes per-program precision of the decision rule. We assess out-of-sample precision using the LOPO triage evaluation in Algorithm 1. Across the 24 programs that have curvature-feature traces (of 38 total), which contain 179 unstable curvature-feature runs, the cross-program aggregate achieves precision 1.00 (TP = 10, FP = 0) and recall 0.056 (10 of 179, FN = 169). We observed that the zero-false-positive property holds out-of-sample, since no stable run was assigned to a high-HVP cluster in our evaluation. LOPO recall is low because the extreme-HVP signature driving C1 ($\sim 5 \times 10^6$) appears concentrated in a few programs. When C1-contributing programs are held out, their unstable runs are assigned to the next-highest-HVP cluster rather than detected. The rule therefore provides reliable precision across programs but limited recall outside the programs that formed C1. Both figures must be reported together. In-sample recall 0.676 and F1 0.807 characterize the rule within a known program subset, and cross-program recall 0.056 characterizes its generalizability.

Precision-recall operating points. The low LOPO recall represents one operating point on a precision-recall trade-off. Fig. 9 shows PR curves under program-held-out evaluation for baseline and baseline+CF classifiers at $k=1$ and $k=5$. At $k=1$, the baseline+CF classifier achieves 0.90 precision at 0.96 recall, indicating that supervised curvature-based models can achieve both high precision and high recall in this setting. The LOPO cluster rule (star) operates at the extreme high-precision end (precision 1.00, recall 0.056), while the in-sample cluster rule (diamond) lies at precision 1.00 with recall 0.676. The operating point depends on the relative cost of false positives vs. missed instabilities.

Mismatch-prevalence variation. Clusters C0 and C5 ($n=1346$ and $n=933$) exhibit mismatch prevalences of 49% and 50%, while C4 ($n=536$) has 0.9%. All three have instability rates

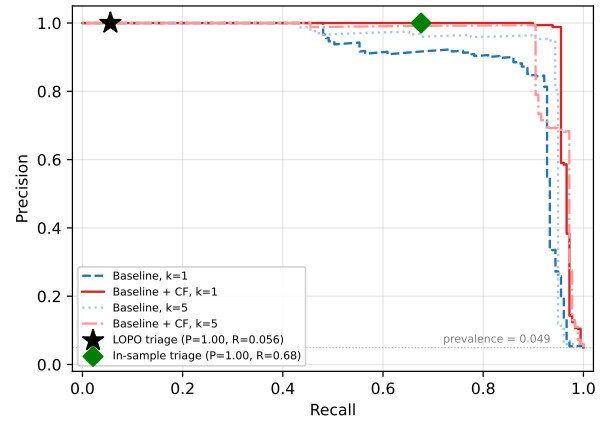


Fig. 9. Instability precision–recall curves under program-held-out evaluation

below 2.3%. This $55\times$ difference in mismatch prevalence, invisible at $K=2$, suggests that *TV-mismatch* monitoring may be needed for some low-curvature program types but not others. These cluster patterns suggest that epoch-0 assignment may help prioritize monitoring. Programs resembling C0 or C5 showed high mismatch prevalence, whereas those resembling C4 did not.

RQ₂ Summary. We found that most instability originates at initialization, with 96% of explosive runs occurring at epoch 0. Incorporating curvature-based features improves cross-program detection (ROC-AUC 0.918 \rightarrow 0.977 at $k=1$). The unsupervised LOPO triage rule provides a high-precision but low-recall operating point, while supervised curvature models offer adjustable precision–recall trade-offs.

Answering RQ₃: Optimizer features for mismatch detection on unseen programs

To answer RQ₃, we compare optimizer features against a loss-and-accuracy baseline for mismatch detection, under both evaluation strategies, on an overlap-controlled program subset and on the full subsets.

Overlap-controlled comparison (primary). The two configurations cover different programs and mismatch prevalences, so we compare them on an overlap-controlled program subset. We therefore interpret absolute CF-vs-OF differences cautiously and focus on within-configuration gaps for the full subsets. Feature availability differs across configurations, so the stable-run sets are not identical. Table VIII reports the results. We observed that curvature features add little discrimination (within-program ROC-AUC 0.816 to 0.816, cross-program 0.730 to 0.731). Optimizer features substantially improve within-program detection (0.899 to 0.971) but slightly reduce cross-program performance relative to the baseline model (0.826 to 0.782). The gap between within and held for the +OF condition is 0.189.

Full-dataset analysis. Table IX reports the same analysis on the full program subsets. The CF subset has 3,278 stable runs across 22 programs at prevalence 0.37, and the OF subset

TABLE VIII
OVERLAP-CONTROLLED T/V -MISMATCH DETECTION ($k=5$)

Config	Features	Setting	n	π	ROC-AUC	PR-AUC
CF	Baseline	within	1317	.50	0.816 [0.618, 0.981]	0.855 [0.659, 0.973]
	Baseline	cross	1317	.50	0.730 [0.475, 0.959]	0.773 [0.441, 0.921]
	+CF	within	1317	.50	0.816 [0.618, 0.981]	0.856 [0.661, 0.974]
	+CF	cross	1317	.50	0.731 [0.476, 0.959]	0.774 [0.442, 0.921]
OF	Baseline	within	410	.42	0.899 [0.704, 0.987]	0.907 [0.637, 0.988]
	Baseline	cross	410	.42	0.826 [0.596, 0.970]	0.830 [0.491, 0.978]
	+OF	within	410	.42	0.971 [0.860, 0.999]	0.957 [0.817, 1.000]
	+OF	cross	410	.42	0.782 [0.434, 0.988]	0.803 [0.444, 0.987]

n = stable runs, π = positive-class prevalence.

has 1,256 stable runs across 26 programs at prevalence 0.51. The two subsets cover different programs, so we focus on within-configuration generalizability gaps. Curvature features add negligible discrimination (within-program 0.799 to 0.799, cross-program 0.738 to 0.738). Optimizer features improve within-program detection (0.874 to 0.897) but degrade substantially under program-held-out evaluation (0.858 to 0.612), a generalizability gap of 0.285. The larger gap in the full dataset relative to the overlap-controlled subset (0.285 vs. 0.189) reflects sensitivity to program composition, as the two subsets cover different programs with different mismatch prevalences (Table IX).

TABLE IX
 T/V -MISMATCH DETECTION AT $k=5$ ON FULL DATASET (STABLE RUNS ONLY)

Config	Features	Setting	n	π	ROC-AUC	PR-AUC
CF	Baseline	within	3278	.37	0.799 [0.657, 0.918]	0.794 [0.611, 0.914]
	Baseline	cross	3278	.37	0.738 [0.577, 0.871]	0.632 [0.410, 0.825]
	+CF	within	3278	.37	0.799 [0.657, 0.919]	0.794 [0.611, 0.914]
	+CF	cross	3278	.37	0.738 [0.577, 0.872]	0.632 [0.411, 0.825]
OF	Baseline	within	1256	.51	0.874 [0.681, 0.972]	0.922 [0.709, 0.987]
	Baseline	cross	1256	.51	0.858 [0.671, 0.949]	0.892 [0.667, 0.974]
	+OF	within	1256	.51	0.897 [0.728, 0.979]	0.916 [0.703, 0.987]
	+OF	cross	1256	.51	0.612 [0.371, 0.846]	0.566 [0.267, 0.873]

n = stable runs, π = positive-class prevalence. Optimizer features show a cross-program generalizability gap of 0.285.

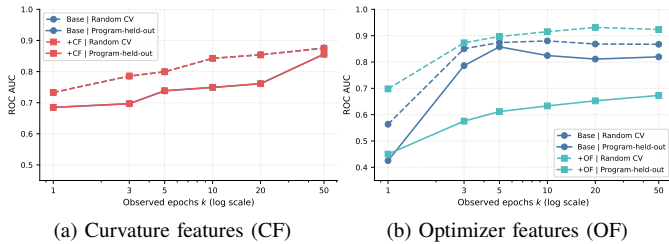


Fig. 10. T/V -mismatch ROC-AUC across observation windows

Fig. 11 shows that the linear model’s optimizer-feature coefficients vary substantially across within-program CV folds, which suggests that these features are being used through

program-specific patterns rather than shared fault semantics. This pattern appears consistent with shortcut learning [10], where classifiers rely on correlations that hold in-distribution but not under shift. This interpretation is consistent with our cross-program results, where activation and optimizer features degraded on unseen programs with different characteristic scales.

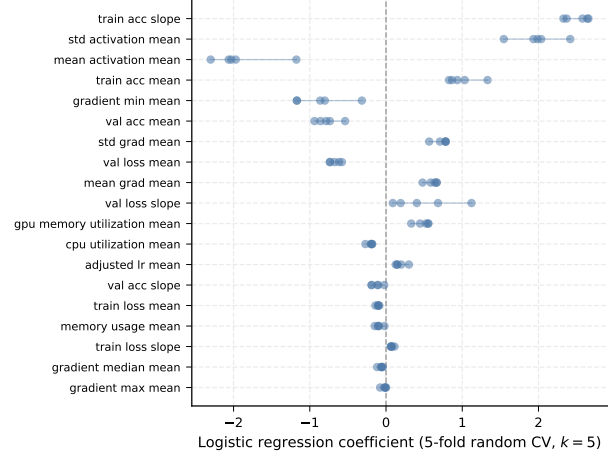


Fig. 11. Optimizer-feature logistic regression coefficients across within-program CV folds

Feature-group ablation. To identify which optimizer-feature groups are most associated with the cross-program degradation, Fig. 12 reports T/V -mismatch ROC-AUC at $k=5$ under program-held-out evaluation after removing each feature group in turn from the full OF channel set (1,256 stable runs, 26 programs). We found that removing activation statistics leads to the largest cross-program improvement (0.627 to 0.696, gap reduction from 0.270 to 0.195), suggesting that per-layer activation scales are a primary source of program-specific shortcut patterns. Removing system resource metrics also narrows the gap (0.270 to 0.236). In contrast, removing gradient statistics or learning rate has minimal effect on cross-program performance. The baseline-only condition (i.e., no OF channels) achieves the smallest gap (0.062) but retains cross-program ROC-AUC of 0.812, suggesting that loss and accuracy metrics alone may provide the most reliable mismatch detection across programs.

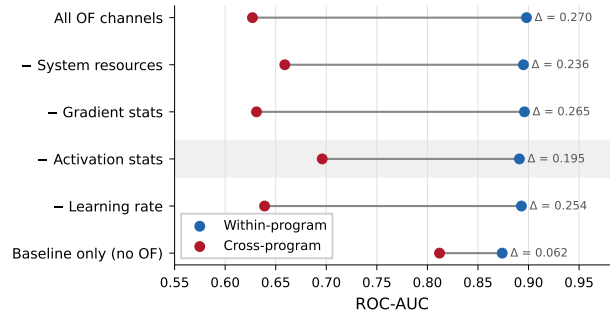


Fig. 12. Feature-group ablation for T/V -mismatch detection at $k=5$

RQ₃ Summary. We found that optimizer features substantially improve within-program *TV-mismatch* detection but degrade under program-held-out evaluation (generalizability gap up to 0.285), driven primarily by per-layer activation statistics. These results reveal an observability–generalizability trade-off introduced by richer runtime features that is not visible under within-program evaluation.

C. Re-evaluation of Existing Techniques

To assess whether the evaluation-strategy gap generalizes beyond our linear methodology, we reimplement the feature extraction code of four existing dynamic-analysis techniques (DEfault [8], DeepFD [7], AutoTrainer [15], and DeepDiagnosis [6]) and evaluate them on DYNFAULT under both settings on the four-class fault-type task at $k=5$. We follow the feature definitions in the original papers [6], [7], [8], [15] and use their provided replication packages. We reproduced the reported accuracy values to within 3% [17].

Learning-based techniques. DEfault features (42 features) and DeepFD features (160 features) are evaluated with both Random Forest (RF) and Logistic Regression (LR). Fig. 13 reports the results. With their original RF classifiers, both techniques achieve within-program accuracy above 0.65 but cross-program accuracy drops to 0.32, a gap of 0.34. This gap is *larger* than the 0.190 observed with logistic regression in RQ1, which suggests that the more expressive RF classifier captures more program-specific structure. Under LR, DEfault features show a gap of 0.088 (within 0.357, cross 0.270), while DeepFD features show a near-zero gap at near-chance performance, which suggests that DeepFD’s 160 statistical features are largely non-discriminative under a linear model.

Rule-based techniques. AutoTrainer and DeepDiagnosis are rule-based detectors that identify the *presence* of training problems (e.g., vanishing gradient, dying ReLU) but do not classify the underlying fault type. AutoTrainer’s five rules trigger on 94.2% and DeepDiagnosis’s eight symptom detectors on 100% of traces in DYNFAULT, indicating that the traces contain the monitored runtime metrics. The rules fire on all fault types without distinction, so they cannot produce fault-type classification metrics, and the evaluation-strategy distinction does not apply to fixed rules.

We found that the evaluation-strategy gap is not an artifact of our linear methodology. It is larger, not smaller, with the higher-capacity RF classifiers used by existing techniques. In our experiments, the gap therefore appears to reflect the cross-program generalization challenge itself rather than a specific classifier or feature set.

D. Discussion and Implications

Our results indicate that evaluation strategy and runtime feature design interact, jointly influencing both measured and actual diagnostic performance. Under within-program CV, we observed that all feature sets benefit from program-specific structure, so their apparent performance levels converge. Only under program-held-out evaluation did the generalizability differences between feature designs become visible in our experiments. This interaction has direct implications for feature

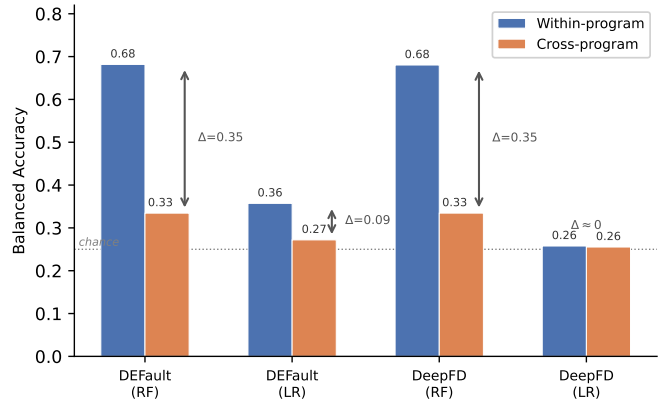


Fig. 13. Within- vs. cross-program accuracy for DEfault and DeepFD at $k=5$

design. Optimizer features improve within-program mismatch detection (ROC-AUC 0.90 to 0.97 on the overlap-controlled subset), but this improvement degrades under program-held-out evaluation (0.78), exposing program-specific shortcuts. Curvature features, by contrast, provided a generalizable instability signal under both strategies in our experiments. We observed that features that appear similarly effective within a program pool may differ substantially when program-specific structure cannot be exploited. The appropriate instrumentation therefore depends on the task. Loss and accuracy features are often sufficient for mismatch detection, whereas curvature features are worth their additional cost when early instability must not be missed. We derive the following implications from these findings.

- Align validation with deployment.** Cross-program claims require program-held-out evaluation [11], [14], since within-program results may overestimate cross-program performance. Reporting program-identity predictability serves as an indicator of program-specific shortcuts.
- Evaluate feature configurations separately.** Additional logging channels can introduce shortcuts detectable only under grouped evaluation [31]. Each feature configuration should be evaluated under program-held-out splits before deployment. Our results indicate that per-program normalization reduces program-identity predictability without degrading cross-program performance, suggesting that normalization-invariant designs may improve transfer.
- Monitor instability at initialization.** In our dataset, 96% of instability occurred at epoch 0, and curvature features generalized under program-held-out evaluation, supporting a high-precision early-termination rule, while supervised models offer adjustable precision–recall in this setting.

V. THREATS TO VALIDITY

External validity. Our findings derive from 38 programs in DYNFAULT with mutation-injected faults. Mutation enables controlled experimentation and the fault categories are grounded in empirical bug taxonomies [2], [19]. Mutants may not capture the full diversity of real-world training failures. We mitigate

optimism by adopting program-held-out evaluation, which explicitly tests generalization to unseen programs, and we treat replication on real-fault corpora as future work to confirm that the gap magnitudes hold beyond mutation-injected faults.

Construct validity. Fault-type labels correspond to the applied mutation operators. The *TV-mismatch* label relies on the corpus-provided `acc_gap_too_big` flag with a fixed threshold [8]. We fixed this threshold to match the DEFault corpus construction protocol and did not tune it per architecture. RNNs, CNNs, and FFNNs differ in expected training/validation gap dynamics, so threshold sensitivity across architecture types should be evaluated in future work. Alternative operationalization may produce different absolute metrics, but the central observation that within-program evaluation reflects program-specific feature structure does not depend on the particular threshold.

Internal and conclusion validity. We use linear models to reduce the risk that classifier capacity dominates the observed effects. Confidence intervals are computed via a cluster bootstrap over programs [29]. With 38 clusters, uncertainty is non-trivial, so we report full intervals and avoid over-interpreting small differences. The CF and OF configurations were collected on partially different program subsets. To reduce this confound, we report both overlap-controlled comparisons on shared programs and within-configuration generalizability gaps on the full subsets. Absolute CF-vs-OF performance levels should therefore be interpreted cautiously.

VI. RELATED WORK

Empirical studies of DL bugs characterize common root causes and failure symptoms, and provide the taxonomies that diagnosis and mutation operators build on [1], [2], [18], [32]. Building on these taxonomies, dynamic-analysis techniques learn from runtime training metrics to detect and diagnose failures. DeepDiagnosis [6] and AutoTrainer [15] implement symptom detectors and repair heuristics for training problems. DeepFD [7] and DEFault [8] frame diagnosis as supervised learning over aggregated runtime metrics, allowing fault-type classification and localization. Qi et al. [9] further augment runtime metrics with coverage-derived metrics. Across this line of work, evaluations measure within-program reuse and, in several cases, detection on real-world fault benchmarks. The cross-program generalization challenge, where the diagnostic model encounters a program with different architecture, dataset, and training dynamics, has not been separately measured. Additional techniques support interactive diagnosis and pre-execution checks. Cockpit [28] and UMLAUT [16] expose gradient distributions, curvature-related signals, and program structure to support human-in-the-loop debugging. DeepLocalize [33] uses dynamic analysis of value propagation between layers to localize faults in DNNs. Hessian-derived metrics have also been used to localize fault sources in attention models [22]. Static analyses for numerical bugs [34] and design-by-contract approaches for DL APIs [35] aim to prevent certain failures before execution.

Many diagnosis studies rely on mutation-injected faults to obtain labeled data at scale. DeepMutation [36] and Deep-

Crime [19] design mutation operators grounded in empirical bug taxonomies. A recent study shows that pre-training mutants better match real faults than post-training mutants under coupling and behavioral-similarity criteria [37], supporting the construct validity of fault-injected corpora. DYNFAULT follows this approach and uses mutation-injected runs to enable controlled measurement of generalization across programs. The need to align validation with deployment is well established in cross-project defect prediction [11], [12], [38], grouped cross-validation for clustered data [13], and operational ML splitting decisions [14], [31], [39]. Separately, shortcut learning [10] explains why rich runtime features can degrade under distribution shift, and curvature-aware analyses [23], [24], [25], [26], [27] motivate curvature-derived signals as transferable instability indicators. Our study connects these threads by measuring the evaluation-strategy gap for DL fault diagnosis and showing that evaluation protocol and feature design interact to determine both measured and actual diagnostic performance.

VII. CONCLUSION

In this work, we studied whether dynamic-analysis fault diagnosis techniques for DL training failures generalize to programs that were not seen during training. Using DYNFAULT, we found that fault-type diagnosis achieved higher balanced accuracy under within-program evaluation than under program-held-out evaluation, with a gap of 0.190. We also observed a similar performance gap across four existing fault diagnosis techniques. Further analysis indicates that program-level structure in the runtime features explains much of this gap, while some fault-related information still generalizes across programs. Our feature analysis shows that gains from richer runtime features do not always transfer to unseen programs. Curvature features helped detect instability on unseen programs. Optimizer and activation features improved training/validation mismatch detection mainly within the same program, with much smaller gains on unseen programs. These findings suggest that within-program evaluation can overestimate diagnostic performance and make richer logging appear more useful than it is for cross-program diagnosis. Future work should assess whether these patterns hold on real-world faults and design methods that help diagnostic models focus on fault-related behavior rather than program-specific runtime patterns.

REFERENCES

- [1] M. J. Islam, G. Nguyen, R. Pan, and H. Rajan, "A comprehensive study on deep learning bug characteristics," in *Proceedings of the 27th ACM Joint European Software Engineering Conference and Symposium on the Foundations of Software Engineering (ESEC/FSE)*, 2019, pp. 510–520. doi: 10.1145/3338906.3338955
- [2] N. Humbaeva et al., "Taxonomy of real faults in deep learning systems," in *Proceedings of the ACM/IEEE 42nd International Conference on Software Engineering (ICSE)*, 2020, pp. 1110–1121. doi: 10.1145/3377811.3380395
- [3] H. Li et al., "Visualizing the loss landscape of neural nets," in *Advances in Neural Information Processing Systems (NeurIPS)*, 2018.
- [4] R. Zhang et al., "An empirical study on program failures of deep learning jobs," in *Proceedings of the ACM/IEEE 42nd International Conference on Software Engineering (ICSE)*, 2020, pp. 1159–1170. doi: 10.1145/3377811.3380362

- [5] M. J. Islam, R. Pan, G. Nguyen, and H. Rajan, "Repairing deep neural networks: Fix patterns and challenges," in *Proceedings of the ACM/IEEE 42nd International Conference on Software Engineering (ICSE)*, 2020, pp. 1135–1146. doi: 10.1145/3377811.3380378
- [6] M. Wardat, B. D. Cruz, W. Le, and H. Rajan, "Deepdiagnosis: Automatically diagnosing faults and recommending actionable fixes in deep learning programs," in *Proceedings of the 44th International Conference on Software Engineering (ICSE)*, 2022, pp. 561–572. doi: 10.1145/3510003.3510071
- [7] J. Cao, Y. Lu, M. Wen, and S. Cheung, "Deepfd: Automated fault diagnosis and localization for deep learning programs," in *Proceedings of the 44th International Conference on Software Engineering (ICSE)*, 2022, pp. 573–585. doi: 10.1145/3510003.3510099
- [8] S. Jahan, M. B. Shah, P. Mahbub, and M. M. Rahman, "Improved detection and diagnosis of faults in deep neural networks using hierarchical and explainable classification," in *Proceedings of the IEEE/ACM 47th International Conference on Software Engineering (ICSE)*, 2025, pp. 2944–2956. doi: 10.1109/ICSE55347.2025.00224
- [9] X. Qi, T. Zhu, and Y. Li, "Coverage-enhanced fault diagnosis for deep learning programs: A learning-based approach with hybrid metrics," *Information and Software Technology*, vol. 173, p. 107488, 2024. doi: 10.1016/j.infsof.2024.107488
- [10] R. Geirhos et al., "Shortcut learning in deep neural networks," *Nature Machine Intelligence*, vol. 2, pp. 665–673, 2020. doi: 10.1038/s42256-020-00257-z
- [11] T. Zimmermann et al., "Cross-project defect prediction: A large scale experiment on data vs. domain vs. process," in *Proceedings of the Joint Meeting of the European Software Engineering Conference and the ACM SIGSOFT International Symposium on the Foundations of Software Engineering*, 2009, pp. 91–100. doi: 10.1145/1595696.1595713
- [12] C. Tantithamthavorn, S. McIntosh, A. E. Hassan, and K. Matsumoto, "An empirical comparison of model validation techniques for defect prediction models," *IEEE Transactions on Software Engineering*, vol. 43, no. 1, pp. 1–18, 2017. doi: 10.1109/TSE.2016.2584050
- [13] D. R. Roberts et al., "Cross-validation strategies for data with temporal, spatial, hierarchical, or phylogenetic structure," *Ecography*, vol. 40, no. 8, pp. 913–929, 2017. doi: 10.1111/ecog.02881
- [14] Y. Lyu et al., "An empirical study of the impact of data splitting decisions on the performance of AIOps solutions," *ACM Transactions on Software Engineering and Methodology*, vol. 30, no. 4, pp. 1–38, 2021. doi: 10.1145/3447876
- [15] X. Zhang, J. Zhai, S. Ma, and C. Shen, "AutoTrainer: An automatic DNN training problem detection and repair system," in *Proceedings of the IEEE/ACM 43rd International Conference on Software Engineering (ICSE)*, 2021, pp. 359–371. doi: 10.1109/ICSE43902.2021.00043
- [16] E. Schoop, F. Huang, and B. Hartmann, "UMLAUT: Debugging deep learning programs using program structure and model behavior," in *Proceedings of the 2021 CHI Conference on Human Factors in Computing Systems (CHI)*, 2021. doi: 10.1145/3411764.3445538
- [17] S. Jahan, *Replication Package for the Evaluation Strategy Gap Study*, <https://github.com/SigmaJahan/Evaluation-Strategy-Gap-Study>, Accessed: 2026-06-24, 2026.
- [18] Y. Yang, T. He, Z. Xia, and Y. Feng, "A comprehensive empirical study on bug characteristics of deep learning frameworks," *Information and Software Technology*, p. 107004, 2022. doi: 10.1016/j.infsof.2022.107004
- [19] N. Humbačová, G. Jahangirova, and P. Tonella, "Deepcrime: Mutation testing of deep learning systems based on real faults," in *Proceedings of the 30th ACM SIGSOFT International Symposium on Software Testing and Analysis (ISSTA)*, 2021, pp. 67–78. doi: 10.1145/3460319.3464825
- [20] J. A. Nelder and R. W. Wedderburn, "Generalized linear models," *Journal of the Royal Statistical Society Series A: Statistics in Society*, vol. 135, no. 3, pp. 370–384, 1972.
- [21] B. Ghorbani, S. Krishnan, and Y. Xiao, "An investigation into neural net optimization via hessian eigenvalue density," in *Proceedings of the International Conference on Machine Learning (ICML)*, 2019, pp. 2232–2241.
- [22] S. Jahan and M. M. Rahman, "Can hessian-based insights support fault diagnosis in attention-based models?" In *Proceedings of the 33rd ACM International Conference on the Foundations of Software Engineering (FSE)*, New York, NY, USA: Association for Computing Machinery, 2025, pp. 676–680. doi: 10.1145/3696630.3728522
- [23] B. A. Pearlmutter, "Fast exact multiplication by the hessian," *Neural Computation*, vol. 6, no. 1, pp. 147–160, 1994. doi: 10.1162/neco.1994.6.1.147
- [24] J. Martens, "Deep learning via hessian-free optimization," in *Proceedings of the 27th International Conference on Machine Learning (ICML)*, 2010, pp. 735–742.
- [25] J. M. Cohen et al., "Gradient descent on neural networks typically occurs at the edge of stability," *arXiv preprint arXiv:2103.00065*, 2021.
- [26] S. Arora, Z. Li, and A. Panigrahi, "Understanding gradient descent on the edge of stability in deep learning," in *Proceedings of the 39th International Conference on Machine Learning (ICML)*, PMLR, 2022, pp. 948–1024.
- [27] J. Gilmer et al., "A loss curvature perspective on training instability in deep learning," *arXiv preprint arXiv:2110.04369*, 2021.
- [28] F. Schneider, F. Dangel, and P. Hennig, "Cockpit: A practical debugging tool for the training of deep neural networks," in *Advances in Neural Information Processing Systems (NeurIPS)*, 2021.
- [29] A. C. Cameron, J. B. Gelbach, and D. L. Miller, "Bootstrap-based improvements for inference with clustered errors," *The Review of Economics and Statistics*, vol. 90, no. 3, pp. 414–427, 2008. doi: 10.1162/rest.90.3.414
- [30] A. Gretton et al., "A kernel two-sample test," *Journal of Machine Learning Research*, vol. 13, no. 25, pp. 723–773, 2012.
- [31] D. Sculley et al., "Hidden technical debt in machine learning systems," in *Advances in Neural Information Processing Systems*, 2015, pp. 2503–2511.
- [32] Y. Zhang et al., "An empirical study on TensorFlow program bugs," in *Proceedings of the 27th ACM SIGSOFT International Symposium on Software Testing and Analysis (ISSTA)*, 2018, pp. 129–140. doi: 10.1145/3213846.3213866
- [33] M. Wardat, W. Le, and H. Rajan, "DeepLocalize: Fault localization for deep neural networks," in *Proceedings of the IEEE/ACM 43rd International Conference on Software Engineering (ICSE)*, 2021, pp. 251–262. doi: 10.1109/ICSE43902.2021.00034
- [34] Y. Zhang et al., "Detecting numerical bugs in neural network architectures," in *Proceedings of the ACM Joint European Software Engineering Conference and Symposium on the Foundations of Software Engineering (ESEC/FSE)*, 2020. doi: 10.1145/3368089.3409720
- [35] S. Ahmed et al., "Design by contract for deep learning apis," in *Proceedings of the 31st ACM Joint European Software Engineering Conference and Symposium on the Foundations of Software Engineering (ESEC/FSE)*, 2023. doi: 10.1145/3611643.3616247
- [36] L. Ma et al., "Deepmutation: Mutation testing of deep learning systems," in *Proceedings of the IEEE 29th International Symposium on Software Reliability Engineering (ISSRE)*, 2018, pp. 100–111. doi: 10.1109/ISSRE.2018.00021
- [37] Z. Ahmed, P. Makedonski, and J. Grabowski, "An empirical study of the realism of mutants in deep learning," *arXiv preprint arXiv:2512.16741*, 2025.
- [38] S. Herbold, A. Trautsch, and J. Grabowski, "A comparative study to benchmark cross-project defect prediction approaches," *IEEE Transactions on Software Engineering*, vol. 44, no. 9, pp. 811–833, 2018. doi: 10.1109/TSE.2017.2724538
- [39] S. Amershi et al., "Software engineering for machine learning: A case study," in *2019 IEEE/ACM 41st International Conference on Software Engineering (ICSE-SEIP)*, 2019. doi: 10.1109/ICSE-SEIP.2019.00042